Applied Catalysis B: Environmental 244 (2019) 559–567

Contents lists available at ScienceDirect

Applied Catalysis B: Environmental

journal homepage: www.elsevier.com/locate/apcatb

A novel NiFe@NC-functionalized N-doped carbon microtubule network derived from biomass as a highly efficient 3D free-standing cathode for Li-CO_2 batteries

Huagen Liang[a,b], Yongliang Zhang[c], Fu Chen[a], Shengyu Jing[c,g,*], Shibin Yin[d], Panagiotis Tsiakaras[e,f,g,*]

[a] Low Carbon Energy Institute, School of Materials Science and Engineering, China University of Mining and Technology, Xuzhou, Jiangsu, 221008, China
[b] Key Laboratory of Coal-Based CO2 Capture and Geological Storage, China University of Mining and Technology, Xuzhou, Jiangsu, 221008, China
[c] School of Information and Control Engineering, China University of Mining and Technology, Xuzhou, Jiangsu, 221008, China
[d] Guangxi Key Laboratory for Electrochemical Energy Materials, Collaborative Innovation Center of Renewable Energy Materials (CICREM), State Key Laboratory of Processing for Non-ferrous Metal and Featured Materials, Guangxi University, Nanning 530004, China
[e] Laboratory of Electrochemical Devices Based on Solid Oxide Proton Electrolytes, Institute of High Temperature Electrochemistry, RAS, Yekaterinburg 620990, Russia
[f] Laboratory of Materials and Devices for Electrochemical Power Industry, Ural Federal University, 19 Mira Str., Yekaterinburg 620002, Russia
[g] Laboratory of Alternative Energy Conversion Systems, Department of Mechanical Engineering, School of Engineering, University of Thessaly, Pedion Areos 38834, Greece

ARTICLE INFO

Keywords:
Li-CO_2 battery
Cathode
3D free-standing
Prussian blue analogues
Biomass carbon

ABSTRACT

Rechargeable Li-CO_2 batteries, which utilize CO_2 into electrochemical energy storage systems, provide a promising strategy for alleviating the greenhouse effect and developing high energy density second batteries. However, problems such as poor battery performance and short cycle life still hinder the development of Li-CO_2 batteries. In this work, a novel three-dimensional free-standing NiFe@NC/PPC cathode is prepared by depositing NiFe-Prussian blue analogues on the surface of pomelo peels (PP) and subsequently calcining at high temperature. The products fully retained the three dimensional porous characteristic of biomass, conducing to mass transfer and diffusion. In addition, the high catalytic activity of NiFe@NC is carried forward. Combined with these two advantages, the Li-CO_2 battery with NiFe@NC/PPC cathode exhibits a superior discharge capacity of 6.8 mA h cm^{-2} and can sustain 109 cycles with a cutoff capacity of 0.25 mA h cm^{-2} at a current density of 0.05 mA cm^{-2}. Overall, this study provides a promising way for the fabrication of environmentally friendly and inexpensive cathodes to improve the performance of Li-CO_2 batteries.

1. Introduction

Carbon dioxide (CO_2) is the main component of the greenhouse gases, which is the culprit leading to global warming. Various methods, such as geological sequestration [1], chemical absorption [2] and so on, have been used to reduce CO_2 emissions. However, these methods are of high energy consumption. Li-CO_2 battery is a new type of electrochemical energy storage system fueled by CO_2, which provides a feasible research idea for the reduction of CO_2 emissions [3,4]. However, in fact, low specific energy density and poor cycle stability are the stumbling blocks for developing high performance Li-CO_2 batteries [5–7].

In order to improve the performance of Li-CO_2 batteries, many efforts have been devoted to develop high active catalysts for Li_2CO_3 decomposition. Zhou et al. [8] used Ru@Super P as the cathode for Li-CO_2 batteries. They proposed that Ru nanoparticles are able to promote the reaction between Li_2CO_3 and carbon instead of the self-decomposition of Li_2CO_3 and thereby lower the charge potential and avoid electrolyte decomposition. The resulted cell delivered a discharge capacity as high as 8229 mA h g^{-1} and showed a coulombic efficiency of 86.2% in the first discharge-recharge cycle. However, Ru is expensive and resource scarce, which is not conducive to commercialization of Li-CO_2 batteries. Zhou et al. [9] prepared Cu/N-doped graphene through a gel-like film synthesis mechanism as the cathode catalyst for Li-CO_2 batteries. The addition of Cu nanoparticles improves the catalytic activity and promotes the reaction between Li_2CO_3 and carbon during charging, resulting a low overpotential of 0.77 V and a good cyclability (50 cycles). Furthermore, they explored Ni nanoparticles/N-doped graphene composite for the cathode of Li-CO_2 batteries [10]. It is found that the interaction between Li/CO_2 and Ni is very strong based on first

* Corresponding authors.
E-mail addresses: jingshengyu@cumt.edu.cn (S. Jing), tsiak@uth.gr (P. Tsiakaras).

https://doi.org/10.1016/j.apcatb.2018.11.075
Received 18 September 2018; Received in revised form 20 November 2018; Accepted 24 November 2018
Available online 26 November 2018

principles, suggesting that the Ni surface can effectively adsorb Li and CO_2; the Ni nanoparticles were served as the active centers for CO_2 reduction and evolution reactions. Most importantly, they investigated the reasons why the Li-CO_2 batteries with the transmission metal catalysts exhibited an excellent reversibility. During the discharge/charge cycle test, the surfaces of transmission metal nanoparticles gradually formed a thin oxide film, which can protect the cathodes from the damage caused by the self-decomposition of Li_2CO_3. Geng et al. prepared, via pyrolysis of ZIF-8, Co single-atom catalysts with four-coordinated N. The Co1-N4 active center promoted the binding strength between CO_2 and the catalysts, as well as facilitating CO_2 activation [11]. Pan et al. investigated the CO_2 reduction reaction activities of M-N-C with five transition metals and they established that Fe and Ni are more active than Co, Mn, and Cr for the reduction of CO_2 to CO [12].

Except metal catalysts, N-doped carbon materials were proved to have good catalytic performance for CO_2 reduction [13–15]. Dai et al. demonstrated that heteroatom B, N-codoped holey graphene could enhance the catalytic activity for CO_2 reduction and evolution reactions [16]. The resulting Li-CO_2 battery with B, N-codoped holey graphene displayed an excellent rate performance, outstanding reversibility, and superb long-term cycling stability, compared with that of primary holey graphene.

In this work, we prepared a composite of NiFe@NC core-shell nanoparticles highly dispersed on the free-standing N-doped carbon microtubule network, which derived from the NiFe-Prussian blue analogues/pomelo peel composite. The resulting NiFe@NC/PPC cathodes endowed Li-CO_2 batteries with low overpotentials, excellent cyclability, and high coulombic efficiency.

2. Experimental section

2.1. Materials preparation

All the employed reagents were of analytical grade without further purification. Fresh pomelos were bought from the supermarket. Before being used, the pomelo skins were peeled-off and left the white inner core, and then washed with deionized water to remove impurities. The pomelo peels were cutted into small wafers with diameter of 16 mm and thickness of 1–2 mm.

NiFe-Prussian blue analogues/pomelo peel (NiFe-PBA/PP) precursors were synthesized through a coprecipitation approach according to international literature [17–19]. More specifically, 0.87 g of Ni $(NO_3)_2{\cdot}6H_2O$ and 1.325 g of $Na_3C_6H_5O_7{\cdot}2H_2O$ were dissolved in deionized water (20 mL) and then added several pieces of pomelo peels to form the solution A. Continuous magnetic stirring and ultrasonication for 2 h to ensure that pomelo peel is fully saturated with the solution. Then 0.6585 g of $K_3[Fe(CN)_6]$ was dissolved in 20 mL of distilled water to form the solution B, which was slowly added into the solution A at room temperature. After the mixture was stirred for 15 min, the obtained mixed solution was aged for 24 h at room temperature. The pomelo peels covered with earth-yellow precipitations were removed, washed with deionized water and ethanol, and then dried under vacuum at 60 °C for 12 h. The as obtained PBA/PP precursors were pyrolyzed at 1000 °C in Ar atmosphere to obtain the final air-electrodes, denoted as NiFe@NC/PPC. The average mass of all NiFe@NC/PPC cathodes was 8–15 mg.

For comparison, a powder of NiFe@NC was prepared by the same process without pomelo peels. The free standing cathodes derived from pomelo peels were pyrolyzed at same temperature, named as PPC (carbonized pomelo peels). The average mass of all PPC cathodes was 5–10 mg.

2.2. Material characterization

The structure of the cathodes was characterized by X-ray diff ;raction (XRD, Bruker D8 Advance) under Cu K_α radiation. The morphology and microstructure of the as-prepared samples were recorded using a (Hitachi SU8200 and SU8010) field-emission scanning electron microscope (SEM) and a (FEI Tecnai-20) transmission electron microscope (TEM). X-ray photoelectron spectroscopy (XPS) analysis was carried out by using a (ESCALAB 250Xi) spectroscope with Al K_α radiation to characterize the chemical compositions. All binding energy values were corrected using the internal standard of the C 1 s peak (284.8 eV) as a reference. The NiFe load content was obtained by simultaneous thermal analysis (TG/DSC, NETZSCH, TAQ600) from ambient to 800 °C under flowing air.

2.3. Electrochemical tests

A CR2025-type coin cell was used to perform the electrochemical tests. The cells were assembled in a glove box filled with Ar (MBRAUN, $H_2O < 0.5$ ppm, $O_2 < 0.5$ ppm). Cell pans were machine drilled with 7xΦ1.0 mm holes in an evenly distributed pattern for CO_2 access. The free-standing PPC or NiFe@NC/PPC cathodes were served as the cathode directly, while fresh Li foil was used as the anode, glass filter (Whatman grade GF/D) was employed as a separator and 1 M $LiCF_3SO_3$ in tetra-ethylene glycol dimethyl ether (TEGDME) solution was used as the electrolyte. For the NiFe@NC/carbon paper (NiFe@NC/CP) and Super P/carbon paper (Super P/CP) cathodes preparation, the Super P carbon powder (Temical) or NiFe@NC catalysts mixed with polyvinylidene fluoride (PVDF) at a mass ratio of 9:1 in N-methyl-2-pyrrolidone (NMP) to form a slurry, then uniformly sprayed on carbon paper (12 mm in diameter; mass loading of 0.8–1.0 mg cm^{-2}) and dried at 80 °C overnight in a vacuum oven. All the assembled Li-CO_2 cells were transferred to a sealed glass bottle filled with 1.0 atm pure CO_2 flowing for the electrochemical tests. The cell performances were evaluated by using a battery testing system (Neware, CT-3008, China) between 2.0 and 4.5 V (vs. Li^+/Li) at room temperature. Before each test, the cells were rested for 5 h in CO_2 atmosphere. All specific capacities of the cathodes were normalized by the total weight of the cathode.

Electrochemical impedance spectroscopy (EIS) and cyclic voltammetry (CV) were performed using a PARSTAT 4000 electrochemical workstation (Princeton, USA) equipped with a frequency response analysis (FRA) module. A signal amplitude of 5 mV in the frequency range of 100 kHz to 10 mHz was applied. The anode was used as the reference and also as the counter electrode, while the cathode was used as the working electrode. The cell impedance would be mainly dominated by the cathodic impedance. Cyclic voltammetry (CV) experiments were conducted at a scan rate of 0.1 mV s^{-1} between 2.0 and 4.5 V vs. Li^+/Li. Cyclic tests were controlled with a cutoff capacity of 0.25 mAh cm^{-2} at a current density of 0.05 mA cm^{-2}.

3. Results and discussion

The synthesis process of the NiFe@NC/PPC cathodes is illustrated in Scheme 1.

Firstly, a large amount of Ni^{2+} ions were absorbed on the surface of the hydrophilic pomelo peels. After adding Fe^{3+}, NiFe-PBA cubes were formed and the color of solution changed from green to bright yellow, and then turned to brown. Finally, the white pomelo peels became brown (Fig. S1). After high temperature calcination, the pomelo peels were carbonized and a porous carbon fiber skeleton was obtained. At the same time, NiFe ions were reduced by carbon [20,21], while the PBA cubes transformed into NiFe@NC nanoparticles with core-shell structures. The finally products were black circles (see Fig. S1), which can be directly used as the cathodes of Li-CO_2 batteries.

Scanning electron microscope (SEM) was employed to characterize the morphology of the NiFe-PBA/PP precursor and the produced NiFe@NC/PPC. As can be seen in Figs. 1a–1c , the NiFe-PBA/PP precursor exhibits a porous structure under a large angle of view, which is composed of plicated microfibers. In detail, the NiFe-PBA with typical cubic shape [22], which evenly dispersed on the surface of the pomelo peel

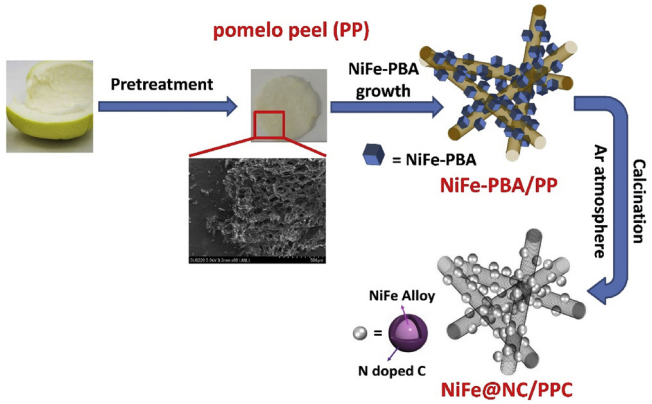

Scheme 1. A schematic of the preparation procedure of NiFe@NC/PPC cathodes.

microfibers. The average size of these NiFe-PBA cubes is approximately 70 nm. It should be noted that NiFe-PBA cubes present a chapped surface, which is mainly caused by spraying gold before SEM testing. As shown in Figs. 1d–1f, the overall morphology of the electrode still maintains the porous structure after calcination, while the pomelo peel turn into carbon microtubules. However, things changed absolutely for NiFe-PBA cubes. The final nanoparticles present an obvious core-shell structure similar to that of frog eggs. We suggest that the relatively open large pore structure formed by interwoven carbon microtubules is beneficial to the diffusion of oxygen and electrolyte, while the micropores formed by the accumulation of NiFe@NC particles contribute to the increase of the three-phase reaction interface. In addition, the carbon layer may be helpful to inhibit the growth and agglomeration of NiFe catalyst in the cell cycle.

The detailed architecture of NiFe@NC/PPC was observed by TEM and it is given in Fig. 2. It is clear to see that the high-resolution TEM image presents the core-shell characteristics of NiFe@NC in Fig. 2a and the calculated interplanar spacing in Fig. 2b is 0.204 nm. The corresponding EDS elemental mapping (Fig. 2c) demonstrates that C, N, Ni and Fe elements are homogeneously distributed throughout the NiFe@NC/PPC electrode. Information for the composition and structure of the as-prepared samples was obtained by X-ray diffraction (XRD). As shown in Fig. S2a, the main diffraction peaks of the Ni-Fe PBA precursor are consistent with the standard patterns of $KNiFe(CN)_6$ (JCPDS: 51-1897), without other miscellaneous peaks, illustrating that the formation of $KNiFe(CN)_6$ is without impurities [22]. In addition, the XRD pattern reveals a broad peak at around $2\theta = 26^\circ$ and a less intense peak at 43° (see Fig. S2b), which matches with the (002) and (101) plane of graphitic C for pomelo peel derived carbon (PPC).

After calcining at 1000 °C, the characteristic peaks of Ni-Fe PBA precursor completely disappear, instead of the diffraction peaks of NiFe alloy (Fig. 3). The peaks at 44.3°, 51.5°, and 75.8° correspond to the (111), (200), and (220) planes of Awaruite phase $FeNi_3$ (JCPDS: 38-0419) respectively, while the characteristic carbon peak at around 26° can be indexed to (002) graphitic plane, deriving from the carbonization of -CN groups in the PBA precursor. Hence, we suggest that Ni-Fe PBA can be successfully converted into NiFe@NC after carbonization treatment. The NiFe@NC/PPC shows both the NiFe@NC and graphite related peaks, which identify the growth of Ni-Fe PBA over pomelo peel. However, the diffraction peaks of NiFe alloy in the composites of

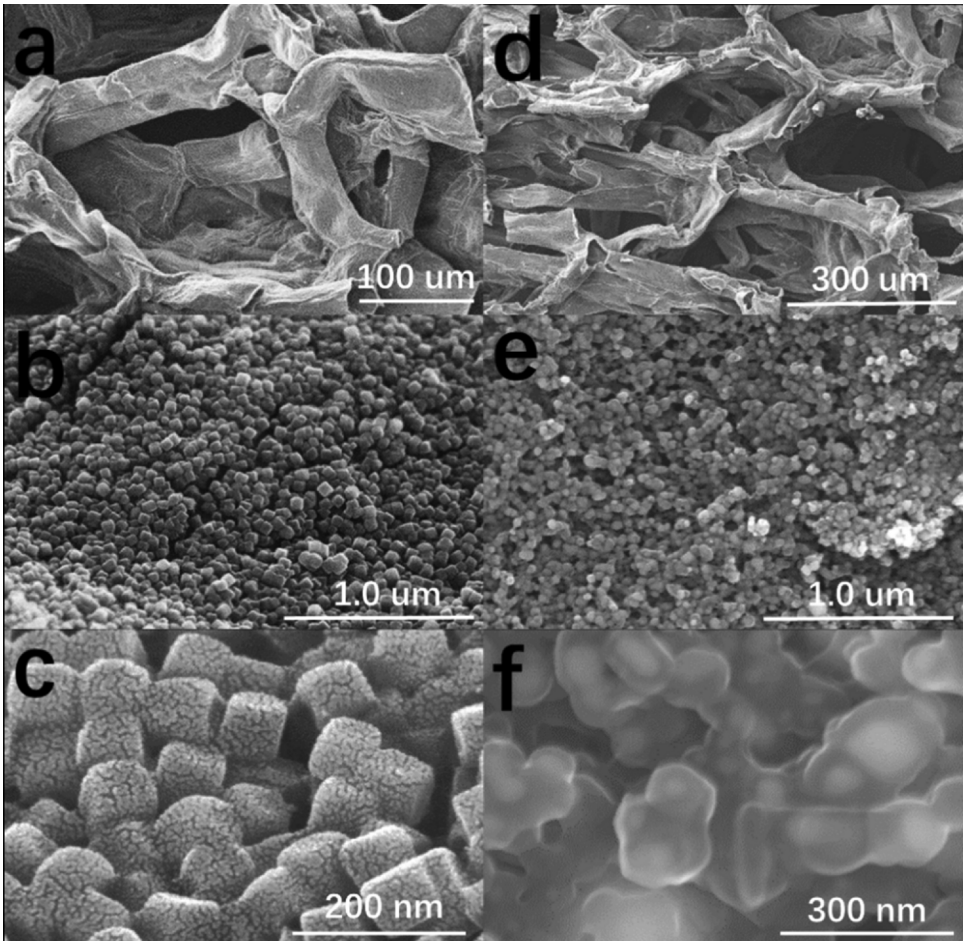

Fig. 1. SEM images of NiFe-PBA/PP precursor (a, b, c) and NiFe@NC/PPC (d, e, f) at different magnifications.

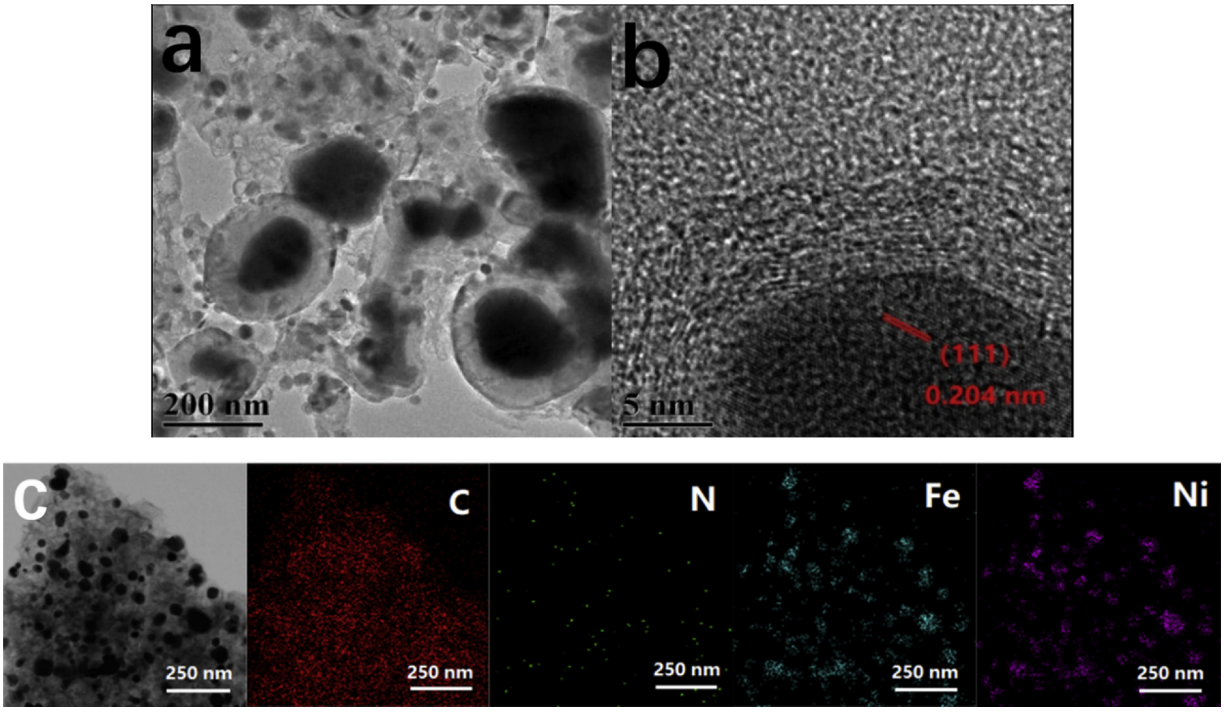

Fig. 2. TEM images of NiFe@NC/PPC (a, b) and EDS mapping of NiFe@NC/PPC (c).

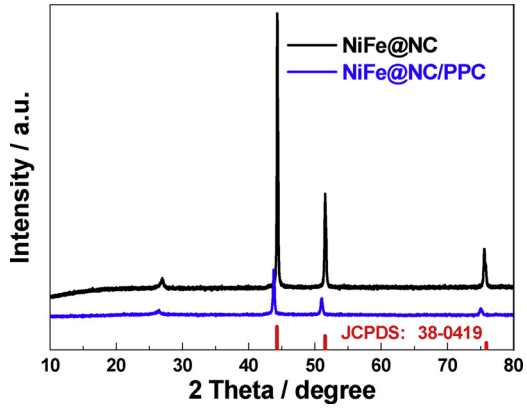

Fig. 3. XRD patterns of NiFe@NC and NiFe@NC/PPC.

NiFe@NC/PPC slightly shift left, implying that there may be a strong interaction between NiFe@NC and PPC, which would promote the CO_2 reduction electrocatalytic activity.

XPS was performed to study the composition and the corresponding chemical valence states of as-prepared samples. The entire XPS spectrum is initially corrected by the high-resolution C 1 s spectrum. From the survey scan spectrum (see Fig. S3), evident peaks for C, N, Ni and Fe are presented. As shown in Fig. 4a, the high-resolution C 1 s XPS spectrum of the fresh NiFe@NC/PPC cathode could be deconvoluted into four peaks at 284.8 eV, 285.2 eV, which can be indexed to carbon in the forms of sp^2 C-sp^2 C and N = sp^2 C, respectively [23–27]. In addition, the high-resolution N 1 s spectrum (Fig. 4b) reveals three components located at 398.0 eV, 399.5 eV and 400.2 eV, corresponding to pyridinic-N, metal-N and pyrrolic-N atom [28,29], respectively. This result demonstrates that the N elements in pomelo peels and the -CN groups in PBA were successfully doped into the carbon skeleton after carbonization, which may be conducive to both the CO_2-reduction reaction (CO_2RR) and evolution reaction (CO_2ER) [16]. As seen in Fig. 4c, it is clear that the binding energy peaks at 870.3 eV and 853.5 eV correspond to Ni° [30–32]. The high-resolution Fe 2p spectrum (Fig. 4d) shows peaks centered at 707.7 eV and 720.7 eV, which can be indexed to Fe° $2p_{3/2}$ [33,34]. Whereas, peaks centered at 725.2 eV assigned to Fe 2p1/2 of Fe(III) and Fe(II), ≈711 eV to ≈713 eV assigned to Fe 2p3/2 of Fe(II) and Fe(III) ions, attributing to the surface oxidation of NiFe@NC nanoparticles.

In-situ cyclic voltammetry (CV) was used to examine the CO_2 catalytic activities of various cathodes in Li-CO_2 batteries from 2 to 4.5 V, as shown in Fig. 5a.

The current density (mA g^{-1}) was normalized to the weight of whole cathode. As disclosed in the cyclic voltammetry (CV) curves, the NiFe@NC/PPC cathode exhibits onset potential of 2.88 V and 3.1 V for positive and negative scan, respectively. The NiFe@NC/CP and NiFe@NC/PPC cathodes almost have similar shape, but the cathodic and anodic peaks for NiFe@NC/PPC cathodes are more obvious and the cathodic current of NiFe@NC/PPC cathodes is much higher.

These results reveal the excellent bi-functional catalytic activity of NiFe@NC/PPC for CO_2 reduction reaction and Li_2CO_3 decomposition. From Fig. 5b and Table S1, it is clear that the R_{ct} of NiFe@NC/PPC is smaller than that of other cathodes, indicating the fast charge transfer process with the combination of NiFe@NC catalyst and PPC support.

The galvanostatic discharge/charge performances of Li-CO_2 batteries with different cathodes were studied at a current density of 0.05 mA cm^{-2}.

As shown in Fig. 6a, the battery with NiFe@NC/PPC cathode shows a stable discharge plateau of ~2.76 V with the corresponding overpotential of ca. 0.04 V [35], while the discharge capacity reaches 6.8 mA h cm^{-2}. The specific capacities of the cathodes is high up to 518 mA h $mg^{-1}_{cathode}$, normalized by the total weight of cathode. More importantly, NiFe@NC/PPC shows a charge capacity of 4.9 mA h cm^{-2} with a perfect columbic efficiency of 72.0%. These results can be favorably compared with the already published ones [5,9,10,36] (see Table 1). As can be distinguished in Fig. 6a, there is a small peak in the charging curve, which also has been reported in other literature reports [35,36]. Although in the literature there is no explanation for this phenomenon, we can speculate as follows: during the discharge process, the non-conductive and insoluble Li_2CO_3 gradually cover the surface of catalysts forming a thick layer (see below Figs. 7a and 7b).

So, we suggest that the most intimate layer of Li_2CO_3, tightly coated

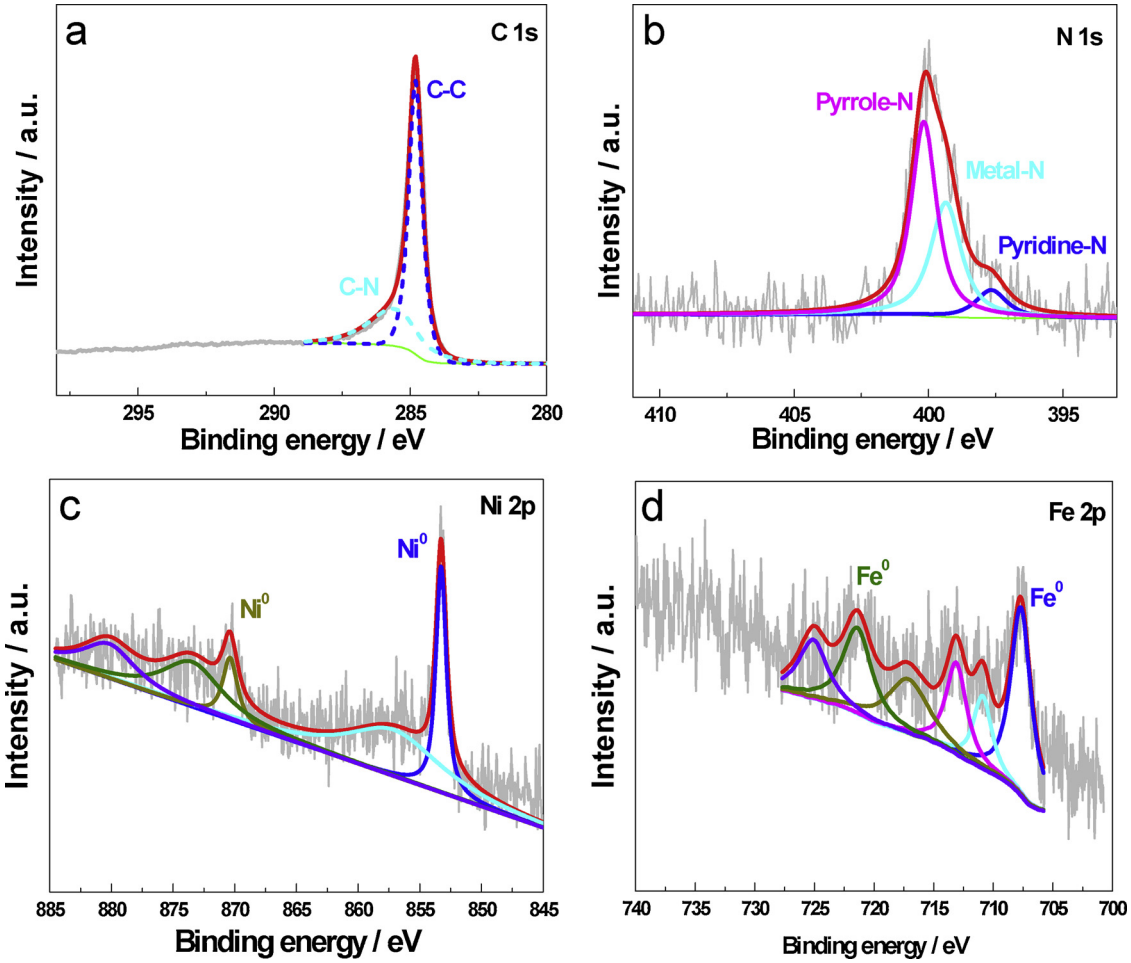

Fig. 4. XPS spectrum of NiFe@NC/PPC.

on the catalysts, is infinitely close to the three phase reaction interface. At the initial stage of charging, the most intimate layer of Li_2CO_3 is easily to be decomposed (voltage < 4.0 V). However, with the continuation of the charging process, a gap formed between catalysts and Li_2CO_3, and these Li_2CO_3 away from the catalyst is hardly to receive electrons. Hence, a greater voltage (> 4.0 V) is needed to decompose the rest Li_2CO_3, similar to breaking the barrier.

In contrast, the electrochemical performance related Super P/CP, NiFe@NC/CP, and individual PPC cathodes were also given. Obviously, the cells with Super P/CP or PPC cathodes show a negligible capacity. Whereas, for NiFe@NC/CP, the electrodes were prepared by coating the slurry of NiFe@NC powder and binder on the carbon paper, resulting a specific capacity as low as 0.4 mA h cm^{-2} and a much higher overpotential compared with that of NiFe@NC/PPC.

In the previous literature [37], it can be found that the pores are mainly distributed in microporous range for catalyst coating method due to the accumulation of catalyst particles, which may cause the CO_2 gas and electrolyte transport channel blocking. Furthermore, the

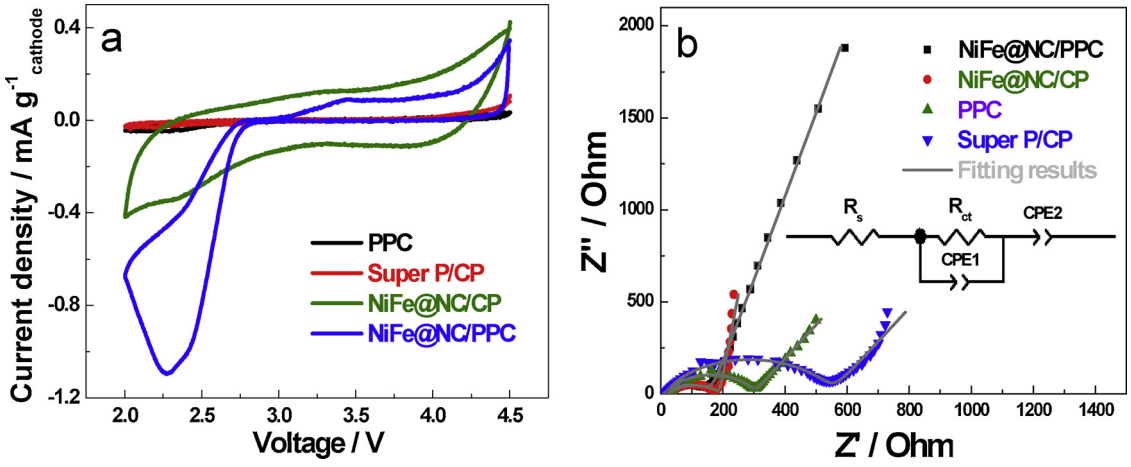

Fig. 5. *In-suit* cyclic voltammetry curves (a) and electrochemical impedance spectra (b) of Li-CO_2 batteries with various cathodes.

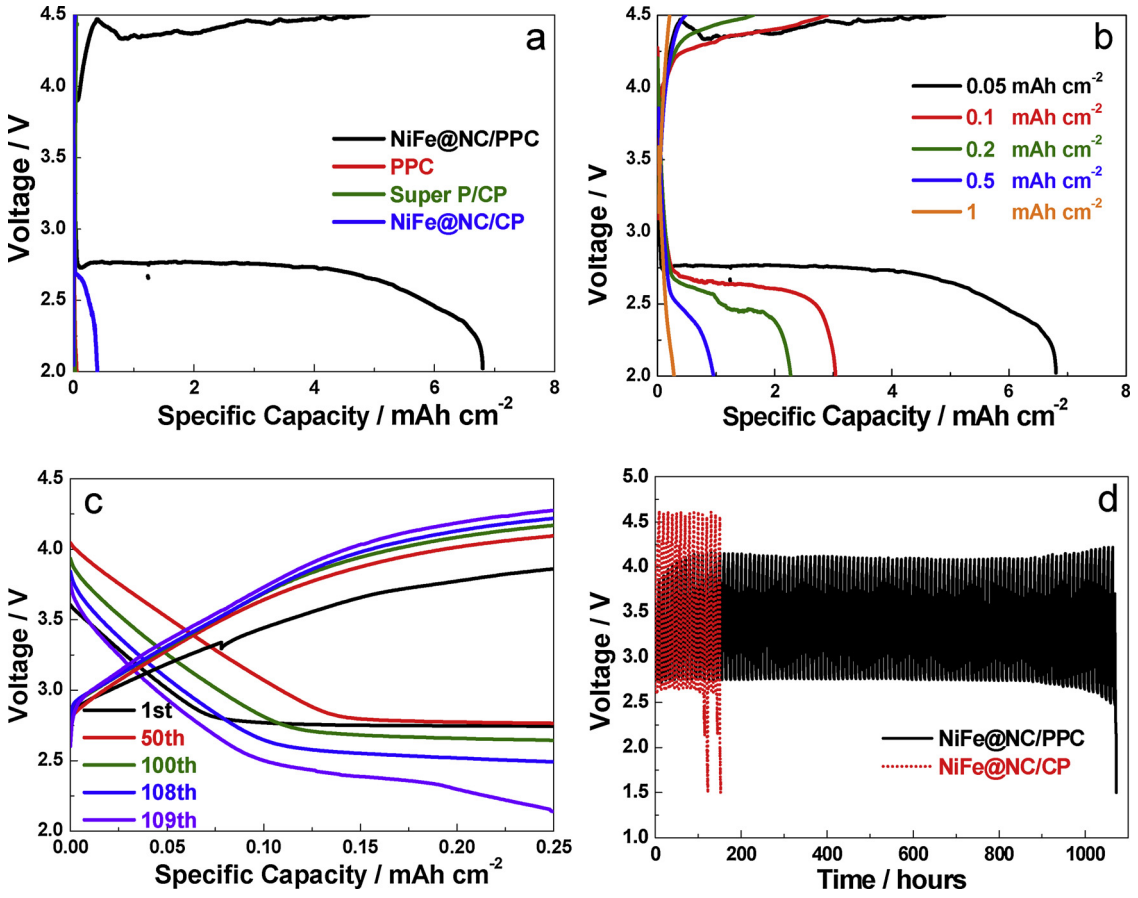

Fig. 6. (a) Charge-discharge curves of Li-CO_2 batteries with various cathodes. (b) Rate capability of NiFe@NC/PPC cathode at different current densities. (c) Cycling stability of NiFe@NC/PPC cathode at 0.05 mA cm^{-2} with a limited capacity of 0.25 mAh cm^{-2}. (d) The variation of the terminal charge and discharge voltages of NiFe@NC/PPC cathode at 0.05 mA cm^{-2}.

generation of insoluble discharged products (Li_2CO_3) will cover on the electrode surface, which further lead to the decrease of the three-phase reaction interfaces [38]. We suggest these are the main reasons for the rapid attenuation in Li-CO_2 battery performance. For PPC cathode, the performance of electrocatalytic CO_2 reduction is poor over N-doped carbon materials, which is consistent with the CV results, leading to a poor cell performance. These results indicate that NiFe@NC/PPC cathodes possess superior electrochemical performances in Li–CO_2 batteries, which might be derived from the synergy of the following advantageous factors: the hybrid materials not only inherit the 3D free-standing structure of PPC and high porosity, but also exhibit high catalytic activity for CO_2 reduction. The plentiful and large channels of NiFe@NC/PPC provide enough volume for the deposition of discharge products, resulting in a more stable electrochemical reaction and an enhanced discharge capacity.

In Fig. 6b, the rate capability is also tested in the voltage window between 2.0 V and 4.5 V. The NiFe@NC/PPC cathode can deliver high specific capacities of 3 mA h cm^{-2} with a columbic efficiency of 95%, even at a higher current density of 0.1 mA cm^{-2}. In addition, the discharge plateau is stable and maintained at 2.64 V. The higher discharge capacity and columbic efficiency further demonstrate that NiFe@NC/PPC cathode possess excellent catalytic activity towards the electrochemical reactions of Li-CO_2 batteries. With the increase of current density, the capacity decreases to 2.3 mA h cm^{-2}, 0.95 mAh cm^{-2} and 0.3 mA h cm^{-2} at current density values of 0.2 mA cm^{-2}, 0.5 mA cm^{-2} and 1 mA cm^{-2}, respectively.

For the exploration of cycle stability, the NiFe@NC/PPC cathodes were measured at a current density of 0.05 mA cm^{-2} with the cut-off capacity of 0.25 mAh cm^{-2}. From Fig. 6c, it is clear that the NiFe@NC/PPC cathodes exhibit a relatively low charge plateau at 3.78 V in the first cycle. Moreover, the discharge plateau maintained at about 2.7 V even after 50 cycles, indicating the excellent catalytic ability for CO_2 reduction and decomposition ability of $LiCO_3$. Interestingly, the discharge platform slightly increased and then reduce with the increase of

Table 1
The performance of Li-CO_2 batteries with different cathodes.

Cathodes	Current density	Specific Capacity (mAh $g^{-1}_{catalyst}$)	Specific Capacity (mAh $g^{-1}_{cathode}$)	Cycle Stability	Refs
Cu/N-G	200 mA g^{-1} (~0.06 mA)	14864	445.9	50	[9]
Ni/N-G	100 mA g^{-1} (~0.03 mA)	17652	529.5	101	[10]
	200 mA g^{-1} (~0.06 mA)	4000	120		
NiO-CNTs	50 mA g^{-1} (~0.015 mA)	9000	270	42	[36]
Ru/Super P	100 mA g^{-1} (~0.05 mA)	8229.5	411.5	70	[8]
B, N-G	300 mA g^{-1} (~0.05 mA)	14996	749.8	200	[16]
Mo_2C/CNT	20 mA (~0.02 mA)	287.5	82.1	40	[35]
NiFe@NC/PPC	**0.05 mA cm^{-2}(~0.04 mA)**		**518**	**109**	**This work**

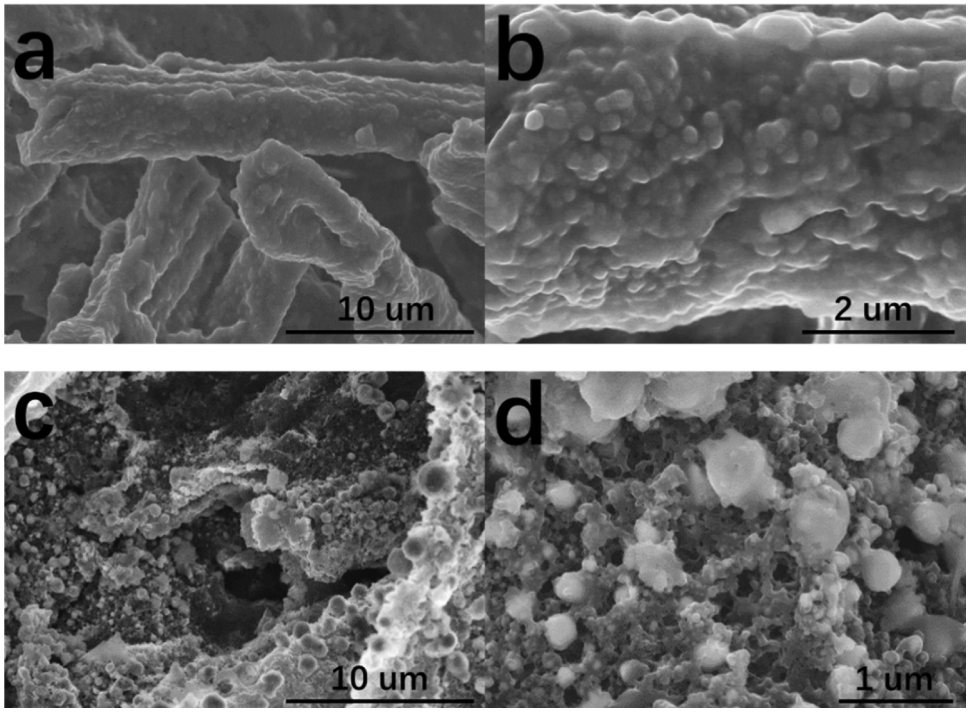

Fig. 7. SEM images of NiFe@NC/PPC cathodes after 1st discharge (a, b), and 1st charge (c, d).

cycling numbers. In the first few cycles, the discharge voltage gradually increased, which may be due to the gradual infiltration of electrolyte and electrode activation process. In the following cycles, the surface of the catalyst was covered by the uncompleted Li_2CO_3 in each cycle, resulting in the decrease of catalyst activity and discharge voltage. The comparison of the cyclic stability of NiFe@NC/PPC and NiFe@NC/CP is presented in Fig. 6d. It is clear that the NiFe@NC/CP could only maintain 13 cycles and the charge potential exceeded 4.5 V. Nevertheless, NiFe@NC/PPC cathodes not only could sustain 109 cycles, but also exhibit lower charge overpotential < 4.3 V even at the ending of cycle testing, which possess enhanced cycle stability in comparison to NiFe@NC/CP.

The reversible formation and decomposition of Li_2CO_3 were investigated by FE-SEM and XPS. As shown in Figs. 7a and 7b, it is clear that the insolubility Li_2CO_3 was deposited on the surface of electrode after discharge to 2.0 V, while the fibrous structure of NiFe@NC/PPC was retained.

After being charged to 4.5 V, almost all of the discharged products disappear and the surface of NiFe@NC/PPC afresh exposes the channels and microporous, as shown in Figs. 7c and 7d. This result indicates the high reversibility of the NiFe@NC/PPC cathode upon cycling. It is believed that the unique porous structure provides sufficient space for Li_2CO_3 deposition and ensures uniform CO_2 transport and electrolyte infiltration, while the excellent catalytic ability enhances the interactions between Li_2CO_3 and NiFe@NC/PPC.

Fig. 8 show the XPS spectra of C 1 s of the NiFe@NC/PPC cathode after the 1st discharge/recharge (Figs. 8a and 8b) and after 100 cycles at limited capacity mode (Figs. 8c and 8d) at 0.05 mA cm^{-2}. Clearly, a sharp peak at 289.8 eV can be observed after 1st discharge, which attributed to the discharge product of Li_2CO_3 (Fig. 8a) [8].

However, the signal of Li_2CO_3 significantly reduced in the XPS spectra of the electrode after recharge (Fig. 8b), indicating that most of the Li_2CO_3 could be decomposed during the recharge process, which demonstrating the good reversibility performance of NiFe@NC/PPC cathode. Yang et al. [8] researched the charging process of Li-CO_2 battery. They believed that Li_2CO_3 would be decomposed only when the charge voltage higher than 4.7 V, without the application of catalyst. At this potential, the electrolyte has been decomposed, and the possibility of battery cycling is zero. The catalyst can reduce the charge voltage and eliminate of superoxide radicals caused by self-decomposition of Li_2CO_3, thus ensuring the battery cycle. This theory also reflects the role of NiFe@NC/PPC, which can promote the occurrence of adverse reactions ($Li + CO_2 \rightleftarrows Li_2CO_3 + C$). To illustrate the reversibility of the battery, the XPS was conducted to investigate the discharge product at the limited capacity cycle mode.

As shown in Figs. 8c and 8d, the XPS peak of Li_2CO_3 maintained a certain intensity after 100th recharge compared with that of discharged cathode after 100th cycle. Therefore, we can infer that a small amount of Li_2CO_3 may be left after the end of each cycle. The accumulation of Li_2CO_3 results in passivation of electrode and blockage of transfer channel for CO_2 and electrolyte, which eventually leads to battery failure.

4. Conclusions

In summary, the discarded biomass (pomelo peels) were used as raw materials and the NiFe-Prussian blue analogues deposited on it to form NiFe-PBA/PP precursor. Followed by carbonization at 1000 °C in Ar atmosphere, the finally obtained 3D free-standing NiFe@NC/PPC cathode was employed as the cathode for Li-CO_2 batteries. SEM images confirmed that this cathode inherits the 3D porous structure of biomass-derived carbon materials, which offer sufficient space for the Li_2O_2 deposition and facilitate mass transport. In addition, this cathode possess high catalytic activity towards CO_2 reduction reaction and Li_2CO_3 decomposition reaction. Benefited from the unique 3D porous characteristics and the superior catalytic activity of the NiFe@NC/PPC composite, Li-CO_2 batteries with NiFe@NC/PPC cathodes delivered high discharge capacity and excellent cyclic stability with stable discharge and charge platforms. XPS analysis revealed that a trace amount of Li_2CO_3 cannot be decomposed in each cycle, which may accumulate on the surface of electrode and cover the catalytic active sites, leading to battery failure.

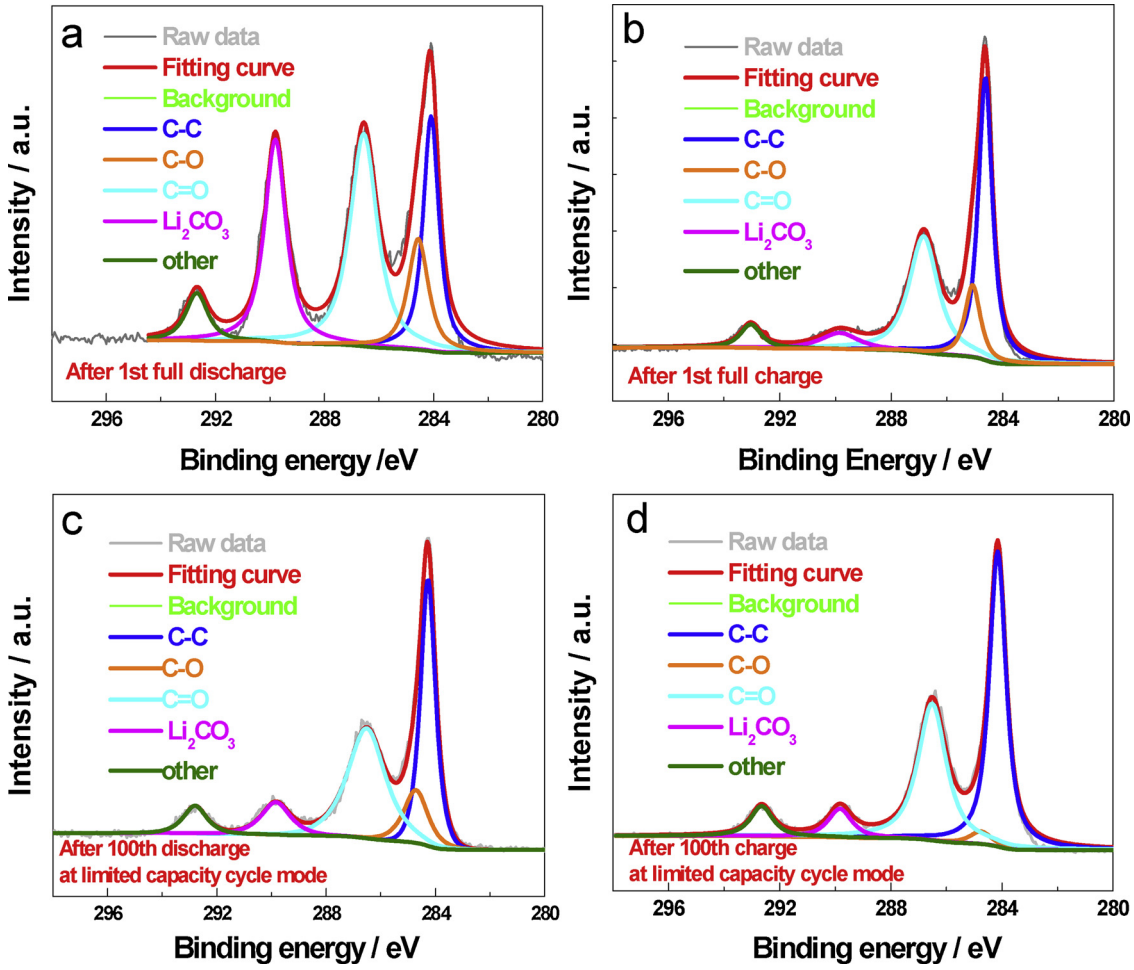

Fig. 8. XPS spectrum of NiFe@NC/PPC cathodes at different discharge/recharge stages.

Acknowledgments

The authors gratefully acknowledge the Fundamental Research Funds for the Central Universities (2015XKMS031) and Natural Science Foundation of Jiangsu Province of China (BK20160239) for financial support of this work. Prof. Tsiakaras has been financially supported by the European Union and Greek national funds through the Operational Program Competitiveness, Entrepreneurship and Innovation, under the call RESEARCH – CREATE – INNOVATE (project code:T1EDK-02442).

Appendix A. Supplementary data

Supplementary material related to this article can be found, in the online version, at doi:https://doi.org/10.1016/j.apcatb.2018.11.075.

References

[1] A.A. Olajire, CO_2 capture and separation technologies for end-of-pipe applications-a review, Energy 35 (2010) 2610–2628.
[2] D.M. D'Alessandro, B. Smit, J.R. Long, Carbon dioxide capture: prospects for new materials, Angew. Chemie Int. Ed. 49 (2010) 6058–6082.
[3] Z. Xie, X. Zhang, Z. Zhang, Z. Zhou, Metal-CO_2 batteries on the road: CO_2 from contamination gas to energy source, Adv. Mater. 29 (2017) 1605891.
[4] X. Zhang, Q. Zhang, Z. Zhang, Y. Chen, Z. Xie, J. Wei, Z. Zhou, Rechargeable Li-CO_2 batteries with carbon nanotubes as air cathodes, Chem. Commun. 51 (2015) 14636–14639.
[5] Z. Zhang, Q. Zhang, Y. Chen, J. Bao, X. Zhou, Z. Xie, J. Wei, Z. Zhou, The first introduction of graphene to rechargeable Li-CO_2 batteries, Angew. Chemie Int. Ed. 54 (2015) 6550–6553.
[6] X. Li, S. Yang, N. Feng, P. He, H. Zhou, Progress in research on Li-CO_2 batteries: mechanism, catalyst and performance, Chin. J. Catal. 37 (2016) 1016–1024.
[7] Y.S. Mekonnen, K.B. Knudsen, J.S.G. Myrdal, R. Younesi, J. Hojberg, J. Hjelm, P. Norby, T. Vegge, Communication: the influence of CO_2poisoning on overvoltages and discharge capacity in non-aqueous Li-Air batteries, J. Chem. Phys. 140 (2014).
[8] S. Yang, Y. Qiao, P. He, Y. Liu, Z. Cheng, J.-J. Zhu, H. Zhou, A reversible lithium-CO_2 battery with Ru nanoparticles as a cathode catalyst, Energy Environ. Sci. 10 (2017) 972–978.
[9] Z. Zhang, Z. Zhang, P. Liu, Y. Xie, K. Cao, Z. Zhou, Identification of cathode stability in Li-CO_2 batteries with Cu nanoparticles highly dispersed on N-doped graphene, J. Mater. Chem. A 6 (2018) 3218–3223.
[10] Z. Zhang, X.-G. Wang, X. Zhang, Z. Xie, Y.-N. Chen, L. Ma, Z. Peng, Z. Zhou, Verifying the rechargeability of Li-CO_2 batteries on working cathodes of Ni nanoparticles highly dispersed on N-doped graphene, Adv. Sci. 5 (2018) 1700567.
[11] Z. Geng, Y. Cao, W. Chen, X. Kong, Y. Liu, T. Yao, Y. Lin, Regulating the coordination environment of Co single atoms for achieving efficient electrocatalytic activity for CO_2 reduction, Appl. Catal. B: Environ. 240 (2018) 234–240.
[12] F. Pan, W. Deng, C. Justiniano, Y. Li, Identification of champion transition metals centers in metal and nitrogen-codoped carbon catalysts for CO_2 reduction, Appl. Catal. B: Environ. 226 (2018) 463–472.
[13] J. Wu, R.M. Yadav, M. Liu, P.P. Sharma, C.S. Tiwary, L. Ma, X. Zou, X.-D. Zhou, B.I. Yakobson, J. Lou, P.M. Ajayan, Achieving highly efficient, selective, and stable CO_2 reduction on nitrogen-doped carbon nanotubes, ACS Nano 9 (2015) 5364–5371.
[14] A. Roy, D. Hursán, K. Artyushkova, P. Atanassov, C. Janáky, A. Serov, Nanostructured metal-N-C electrocatalysts for CO_2 reduction and hydrogen evolution reactions, Appl. Catal. B: Environ. 232 (2018) 512–520.
[15] H.-R.M. Jhong, C.E. Tornow, B. Smid, A.A. Gewirth, S.M. Lyth, P.J.A. Kenis, A nitrogen-doped carbon catalyst for electrochemical CO_2 conversion to CO with high selectivity and current density, ChemSusChem 10 (2017) 1094–1099.
[16] L. Qie, Y. Lin, J.W. Connell, J. Xu, L. Dai, Highly rechargeable lithium-CO_2 batteries with a boron- and nitrogen-Co doped holey-graphene cathode, Angew. Chemie Int. Ed. 56 (2017) 6970–6974.
[17] W. Ahn, M.G. Park, D.U. Lee, M.H. Seo, G. Jiang, Z.P. Cano, F.M. Hassan, Z. Chen, Hollow multivoid nanocuboids derived from ternary Ni-Co-Fe prussian blue analog for dual-electrocatalysis of oxygen and hydrogen evolution reactions, Adv. Funct. Mater. 28 (2018) 1802129.
[18] A. Azhar, M.B. Zakaria, E.M. Ebeid, T. Chikyow, Y. Bando, A.A. Alshehri, Y.G. Alghamdi, Z.X. Cai, N.A. Kumar, J. Lin, H. Kim, Y. Yamauchi, Synthesis of hollow Co-Fe prussian blue analogue cubes by using silica spheres as a sacrificial

template, ChemistryOpen 7 (2018) 599–603.
[19] A. Kumar, S. Bhattacharyya, Porous NiFe-oxide nanocubes as bifunctional electrocatalysts for efficient water-splitting, ACS Appl. Mater. Interfaces 9 (2017) 41906–41915.
[20] Y. Yang, Z. Lun, G. Xia, F. Zheng, M. He, Q. Chen, Non-precious alloy encapsulated in nitrogen-doped graphene layers derived from MOFs as an active and durable hydrogen evolution reaction catalyst, Energy Environ. Sci. 8 (2015) 3563–3571.
[21] S.G. Peera, J. Balamurugan, N.H. Kim, J.H. Lee, Sustainable synthesis of Co@NC core shell nanostructures from metal organic frameworks via mechanochemical coordination self-assembly: an efficient electrocatalyst for oxygen reduction reaction, Small 14 (2018) 1800441.
[22] H.-H. Zou, C.-Z. Yuan, H.-Y. Zou, T.-Y. Cheang, S.-J. Zhao, U.Y. Qazi, S.-L. Zhong, L. Wang, A.-W. Xu, Bimetallic phosphide hollow nanocubes derived from a prussian-blue-analog used as high-performance catalysts for the oxygen evolution reaction, Catal. Sci. Technol. 7 (2017) 1549–1555.
[23] M. Zhong, X. Zhang, D.-H. Yang, B. Zhao, Z. Xie, Z. Zhou, X.-H. Bu, Zeolitic imidazole framework derived composites of nitrogen-doped porous carbon and reduced graphene oxide as high-efficiency cathode catalysts for Li-O_2 batteries, Inorg. Chem. Front. 4 (2017) 1533–1538.
[24] Z. Zhang, J. Bao, C. He, Y. Chen, J. Wei, Z. Zhou, Hierarchical carbon–nitrogen architectures with both mesopores and macrochannels as excellent cathodes for rechargeable Li–O_2 batteries, Adv. Funct. Mater. 24 (2014) 6826–6833.
[25] D. Kong, W. Yuan, C. Li, J. Song, A. Xie, Y. Shen, Synergistic effect of Nitrogen-doped hierarchical porous carbon/graphene with enhanced catalytic performance for oxygen reduction reaction, Appl. Surf. Sci. 393 (2017) 144–150.
[26] H. Gong, H. Xue, T. Wang, H. Guo, X. Fan, L. Song, W. Xia, J. He, High-loading nickel cobaltate nanoparticles anchored on three-dimensional N-doped graphene as an efficient bifunctional catalyst for lithium-oxygen batteries, ACS Appl. Mater. Interfaces 8 (2016) 18060–18068.
[27] Z. Zhang, L. Su, M. Yang, M. Hu, J. Bao, J. Wei, Z. Zhou, A composite of Co nanoparticles highly dispersed on N-rich carbon substrates: an efficient electrocatalyst for Li-O_2 battery cathodes, Chem. Commun. 50 (2014) 776–778.
[28] X. Zeng, C. You, L. Leng, D. Dang, X. Qiao, X. Li, Y. Li, S. Liao, R.R. Adzic, Ruthenium nanoparticles mounted on multielement co-doped graphene: an ultra-high-efficiency cathode catalyst for Li-O_2 batteries, J. Mater. Chem. A 3 (2015) 11224–11231.
[29] S.N. Faisal, E. Haque, N. Noorbehesht, W. Zhang, A.T. Harris, T. Church, A.I. Minett, Pyridinic and graphitic nitrogen-rich graphene for high-performance supercapacitors and metal-free bifunctional electrocatalysts for ORR and OER, RSC Adv. 7 (2017) 17950–17958.
[30] J. Zhu, M. Xiao, Y. Zhang, Z. Jin, Z. Peng, C. Liu, S. Chen, J. Ge, W. Xing, Metal–organic framework-induced synthesis of ultrasmall encased NiFe nanoparticles coupling with graphene as an efficient oxygen electrode for a rechargeable Zn–air battery, ACS Catal. 6 (2016) 6335–6342.
[31] Y. Feng, X.-Y. Yu, U. Paik, N-doped graphene layers encapsulated NiFe alloy nanoparticles derived from MOFs with superior electrochemical performance for oxygen evolution reaction, Sci. Rep. 6 (2016) 34004.
[32] J. Wang, S. Mao, Z. Liu, Z. Wei, H. Wang, Y. Chen, Y. Wang, Dominating role of Ni-0 on the, interface of Ni/NiO for enhanced hydrogen evolution reaction, ACS Appl. Mater. Interfaces 9 (2017) 7139–7147.
[33] S.H. Ahn, X. Yu, A. Manthiram, Wiring" Fe-N-x-embedded porous carbon framework onto 1D nanotubes for efficient oxygen reduction reaction in alkaline and acidic media, Adv. Mater. 29 (2017) 1606534.
[34] M. Li, T. Liu, X. Bo, M. Zhou, L. Guo, A novel flower-like architecture of FeCo@NC-functionalized ultra-thin carbon nanosheets as a highly efficient 3D bifunctional electrocatalyst for full water splitting, J. Mater. Chem. A 5 (2017) 5413–5425.
[35] Y. Hou, J. Wang, L. Liu, Y. Liu, S. Chou, D. Shi, H. Liu, Y. Wu, W. Zhang, J. Chen, Mo2C/CNT: an efficient catalyst for rechargeable Li-CO_2 batteries, Adv. Funct. Mater. 27 (2017) 1700564.
[36] X. Zhang, C. Wang, H. Li, X.-G. Wang, Y.-N. Chen, Z. Xie, Z. Zhou, High performance Li-CO_2 batteries with NiO-CNT cathodes, J. Mater. Chem. A 6 (2018) 2792–2796.
[37] S. Jing, M. Zhang, H. Liang, B. Shen, S. Yin, X. Yang, Facile synthesis of 3D binder-free N-doped carbon nanonet derived from silkworm cocoon for Li-O_2 battery, J. Mater. Sci. 53 (2018) 4395–4405.
[38] L. Liu, H. Guo, Y. Hou, J. Wang, L. Fu, J. Chen, H. Liu, J. Wang, Y. Wu, A 3D hierarchical porous Co_3O_4 nanotube network as an efficient cathode for rechargeable lithium-oxygen batteries, J. Mater. Chem. A 5 (2017) 14673–14681.